

1 GROWTH OF A SINKHOLE IN A SEISMIC ZONE OF THE NORTHERN APENNINES (ITALY)

2 Alessandro La Rosa<sup>1,2</sup>, Carolina Pagli<sup>2</sup>, Giancarlo Molli<sup>2</sup>, Francesco Casu<sup>3</sup>, Claudio De Luca<sup>3</sup>, Amerino  
3 Pieroni<sup>4</sup> and Giacomo D'amato Avanzi<sup>2</sup>

4

5 <sup>1</sup> Dipartimento di Scienze della Terra, Università degli Studi di Firenze, Via G. La Pira, 4, 50121 Firenze, Italy

6 <sup>2</sup> Dipartimento di Scienze della Terra, Università di Pisa, Via S. Maria, 53, 56126 Pisa, Italy

7 <sup>3</sup> CNR, Consiglio Nazionale delle Ricerche, Istituto per il Rilevamento Elettromagnetico dell'Ambiente (IREA-  
8 CNR), Via Diocleziano, 328, 80124 Napoli, Italy

9 <sup>4</sup> Pro.Geo. s.r.l. Via Valmaira, 14, 55032, Castelnuovo di Garfagnana, Italy

10


11 **Keywords:** Sinkhole, InSAR, Seismicity

12 **Abstract**


13 Sinkhole collapse is a major hazard causing substantial social and economic losses. However,  
14 the surface deformations and sinkhole evolution are rarely recorded, as these sites are known  
15 mainly after a collapse, making the assessment of sinkholes-related hazard challenging.  
16 Furthermore, more than 40% of the sinkholes of Italy are in seismically hazardous zones; it remains  
17 unclear whether seismicity may trigger sinkhole collapse. Here we use a multidisciplinary dataset of  
18 InSAR, surface mapping and historical records of sinkhole activity to show that the Prà di Lama lake  
19 is a long-lived sinkhole that was formed over a century ago in active fault zone and grew through  
20 several events of unrest characterized by episodic subsidence and lake-level changes. Moreover,  
21 InSAR shows that continuous aseismic subsidence at rates of up to 7.1 mm yr<sup>-1</sup> occurred during  
22 2003-2008, between events of unrest. Earthquakes on the major faults near the sinkhole are not a  
23 trigger to sinkhole activity but small-magnitude earthquakes at 4-12 km depth occurred during  
24 sinkhole unrest in 1996 and 2016. We interpret our observations as evidence of seismic creep in an  
25 active fault zone at depth causing fracturing and ultimately leading to the formation and growth of  
26 the Prà di Lama sinkhole.

27

## 28 1. Introduction

29 Sinkholes are closed depressions with internal drainage typically associated with karst  
30 environments, where the exposed soluble rocks are dissolved by circulating ground water  
31 (dissolution sinkholes) but other types of sinkholes also exist. Subsidence sinkholes, for example,  
32 can form for both internal erosion and dissolution of covered layers leading to downward  
33 gravitational deformations such as collapse, sagging or suffosion (*Ford and Williams, 2007; Gutiérrez*  
34 *et al., 2008; Gutiérrez et al., 2014*). Deep sinkholes have been often observed along seismically active  
35 faults indicating a causal link between sinkhole formation and active tectonics (*Faccenna et al.,*  
36 *1993; Closson et al., 2005; Florea, 2005; Harrison et al., 2002; Del Prete et al., 2010; Parise et al.,*  
37 *2010; Wadas et al., 2017*). In some cases, the processes responsible for the formation of these  
38 sinkholes have been attributed to fracturing and increased permeability in the fault damage zone  
39 promoting fluid circulation and weathering of soluble rocks at depth. Additionally, when carbonate  
40 bedrocks lie below thick non-carbonate formations, stress changes caused by faulting may cause  
41 decompression of confined aquifers favouring upward migration of deep fluids hence promoting  
42 erosion and collapses (e.g. *Harrison et al., 2002; Wadas et al., 2017*). Seismically-induced stress  
43 changes could also trigger collapse of unstable cavities as in the case of the two sinkholes that  
44 formed near En Gedi (Dead Sea) following the  $M_w$  5.2 earthquake on the Dead Sea Transform Fault  
45 in 2004 (*Salamon, 2004*). Sinkhole subsidence and collapses are a major hazard and cause  
46 substantial economic and human losses globally (*Frumkin and Raz, 2001; Wadas, 2017; Closson,*  
47 *2005*). 

48 In Italy, a total of 750 sinkholes have been identified and the 40% of them are along active  
49 faults (*Caramanna et al., 2008*) but this number could be underestimated due to the high frequency  
50 of sinkholes both related to karst and anthropogenic origin (*Parise and Vennari, 2013*). Seismicity

51 induced sinkhole deformation have been often observed in Italy (e.g. *Parise et al., 2010; Kawashima*  
52 *et al., 2010; Santo et al., 2007*). 

53 The sinkhole of Prà di Lama, near the ~~Pieve Fosciana town (Lucca, Italy)~~, is a quasi-circular  
54 depression filled by a lake. Prà di Lama is located in the seismically active Apennine range of  
55 Northern Tuscany, at the intersection between two active faults (Fig. 1). Hot springs are also present  
56 at Pieve Fosciana suggesting that fluid migration along the faults planes occurs. Sudden lake-level  
57 changes of up to several meters, ground subsidence, surface fracturing and seismicity have occurred  
58 repeatedly since at least 991 A.D. (*Nisio, 2008*). The most recent deformation events occurred in  
59 March 1996 and between May 2016 and October 2017. However, the processes that control the  
60 growth of the Prà di Lama sinkhole remain unclear. Furthermore, whether seismicity along the  
61 active faults around Prà di Lama may trigger sinkhole subsidence or collapse is debated.

62 In this paper we combine recent InSAR observations, seismicity, and surface mapping, as well  
63 as historical records of lake-level changes and ground subsidence at the Prà di Lama from 1828 to  
64 understand the mechanisms of sinkhole growth in an active fault system.

## 65 **2. Geological setting**

66 The area of the Prà di Lama sinkhole is located within the Garfagnana basin (Fig.1), an  
67 extensional graben in the western Northern Apennines, a NW-SE trending fold-and-thrust belt  
68 formed by the stack of different tectonic units caused by the convergence of the Corsica-European  
69 and Adria plates. The current tectonic regime of the Apennines is characterized by shortening in the  
70 eastern sector of the Apennine range and extension in the westernmost side of the range (*Elter et*  
71 *al., 1975; Patacca and Scandone, 1989; Bennett et al., 2012*). The contemporaneous eastward  
72 migration of shortening and upper plate extension are believed to be caused by the roll-back  
73 subduction during the counter-clockwise rotation of the Adria plate (*Doglioni, 1991; Meletti et al.,*  
74 *2000; Serpelloni et al., 2005; Faccenna et al., 2014; Le Breton et al., 2017*). Extension started 4-5 Ma

75 ago leading to the formation of several NW-SE-oriented grabens, bounded by NE-dipping and SW-  
76 dipping normal faults that are dissected by several NE-trending, right-lateral strike-slip faults (Fig.  
77 1). The inner northern Apennines are a seismically active area, where several earthquakes with  $M_w$   
78 > 5 occurred, including the largest instrumentally recorded earthquake,  $M_w$  6.5, in 1920 (*Tertulliani*  
79 *and Maramai, 1998; Rovida et al., 2016; Bonini et al., 2016*) and the most recent  $M_w$  5.1 earthquake  
80 in 2013 (*Pezzo et al., 2014; Stramondo et al., 2014; Molli et al., 2016*).

81 The uppermost stratigraphy at Prà di Lama consists of an 8m-thick layer of alluvial and  
82 palustrine gravels and sandy deposits containing **pity levels**, covering an ~85m-thick sandy-to-silty  
83 fluvio-lacustrine deposits with low permeability (from Villafranchian to present age) (*Chetoni, 1995*)  
84 (Fig.2a and b). These deposits cover a ~1000m-thick turbiditic sequence (Macigno Fm). Below it, a  
85 sequence of carbonate rocks pertaining to the Tuscan Nappe Unit is present reaching down to a  
86 depth of ~2000 m, where anhydrites (Burano fm.) and calcareous-dolomitic breccias (Calcare  
87 Cavernoso Fm.) overlie the Tuscan Metamorphic Units (Fig. 2c).

88 The Prà di Lama lake lies at the centre of a depression (Fig. 2 and 5). The low slopes  
89 characterizing the topography of the area results in the absence of active gravitational ground  
90 motions (Fig 2). Furthermore, the Prà di Lama sinkhole is an isolated feature in the region being the  
91 only mapped sinkhole in the entire Garfagnana graben (*Caramanna et al., 2008*); the closest  
92 sinkhole is in Camaione (Lucca) near the Tuscany coast (Fig.1).

93 The Prà di Lama sinkhole is located at the intersection between two seismically active faults:  
94 the Corfino normal fault (*Di Naccio et al., 2013; Itacha working group, 2003; ISIDE working group,*  
95 **20**) and the right-lateral strike-slip fault M.Perpoli-T.Scoltenna that recently generated the  $M_w$   
96 4.8 earthquake in January 2013 (Fig.1) (*Vannoli, 2013; Pinelli, 2013; Molli et al., 2017*). Hot water  
97 springs are also present at Prà di Lama (*Bencini et al., 1977; Gherardi and Pierotti, 2018*).  
98 Geochemical analyses of the Prà di Lama spring waters by *Gherardi and Pierotti (2018)*, expanding

99 on previous research (*Baldacci et al., 2007*), suggest that both shallow and deep aquifers are present  
100 below Prà di Lama (Fig. 2b). Shallow aquifers have low salinity and low temperature while waters  
101 feeding the thermal springs have high temperature (~57 °C) and high salinity (5.9g/kgw), suggesting  
102 the presence of a deep aquifer at ~2000 m into the anhydrite and the calcareous-dolomitic breccia.  
103 The high salinity of the deep groundwaters is associated with dissolution of the deep evaporitic  
104 formations. Furthermore, un-mixing of deep and shallow waters is interpreted by *Gherardi and*  
105 *Pierotti (2018)* as an evidence of their rapid upwelling likely occurring along the existing faults.

### 106 **3. Data**

107 Century-scale historical records of sinkhole activity are available at Prà di Lama and allow us  
108 to determine the timescale of sinkhole evolution as well as to characterize the different events of  
109 unrest, in particular the two most recent events in 1996 and 2016. InSAR time-series analysis is also  
110 carried out to measure ground deformations in the Prà di Lama sinkhole in the time period between  
111 events of unrest. Finally, the local catalogue of seismicity (ISIDE catalogue, INGV) is used to inform  
112 us on the timing and types of brittle failures in the area of the sinkhole.

#### 113 **3.1 Historical Record**

114 The first historical record of the Prà di Lama sinkhole dates back to the 991 A.D., when the  
115 area was described as a seasonal shallow pool fed by springs. Since then, the depression grew and  
116 several events of unrest consisting of fracturing and fluctuations of the lake level were reported  
117 (*Raffaelli, 1869; De Stefani, 1879, Giovannetti, 1975*) (Table 1). In particular, eight events of unrest  
118 were reported, giving an average of 1 event of ~~unrest~~ every 26 years. We conducted direct  
119 observation of surface deformation around the lake for the two most recent events in 1996 and  
120 2016.

121 In 1996, the lake level experienced a fall of up to 4 m (Fig. 3 and Fig. S1) and at the same time  
122 the springs outside the lake suddenly ~~increase~~ the water outflow. Clay and mud were also ejected

123 by the springs outside the lake while fractures and slumps occurred within the lake due to the water  
124 drop (Fig. 3 and Fig. S1). The unrest lasted approximately 2 months, from March to April 1996.  
125 During the final stages, the water level in the lake rose rapidly ~~recovering its initial level~~ and  
126 contemporaneously the springs water flow reduced.

127 In June 2016, an event of unrest consisting of ground subsidence on the western and southern sides  
128 of the Prà di Lama lake started and lasted approximately 9 months, until February 2017. During this  
129 period fractures formed and progressively grew, increasing their throw to up to 70 cm and affecting  
130 a large area on the western side of the lake (Fig. 3 and Fig. S2). Subsidence around the lake resulted  
131 in an increase of the lake surface in particular on the western side and formation of tensile fractures  
132 (Fig. 3 and Fig. S2). Unlike the 1996 events of unrest, no lake level changes or increase of water flow  
133 from the springs around the lake were observed.

### 134 **3.2 InSAR**

135 InSAR is ideally suited to monitor localized ground deformation such as caused by sinkholes  
136 as it can observe rapidly evolving deformation of the ground at high spatial resolution (*Baer et al.,*  
137 *2002; Castañeda et al., 2009; Atzori et al., 2015; Abelson et al., 2017*). Furthermore, the availability  
138 of relatively long datasets of SAR images in the Apennine allows us to study the behaviour of the  
139 Prà di Lama sinkhole using multi-temporal techniques. We processed a total of 200 interferograms  
140 using SAR images acquired by the ENVISAT satellite between 2003 to 2010 from two distinct tracks  
141 in Ascending or Descending viewing geometry (tracks 215 and 437). We used the Small BAseLine  
142 Subset (SBAS) multi-interferogram method originally developed by *Berardino et al. (2002)* and  
143 recently implemented for parallel computing processing (P-SBAS) by *Casu et al. (2014)* to obtain  
144 incremental and cumulative time-series of InSAR Line-of-Sight (LOS) displacements as well as maps  
145 of average LOS velocity. In particular, the InSAR processing has been carried out via the ESA platform

146 P-SBAS open-access on-line tool named G-POD (Grid Processing On Demand) that allows generating  
147 ground displacement time series from a set of SAR data (*De Luca et al., 2015*).

148 The P-SBAS G-POD tool allows the user to set some key parameters to tune the InSAR  
149 processing. In this work, we set a maximum perpendicular baseline (spatial baseline) of 400 m and  
150 maximum temporal baseline of 1500 days. The geocoded pixel dimension was set to ~80 m by 80 m  
151 (corresponding to averaging together 20 pixels in range and 4 pixels in azimuth).

152 We initially set a coherence threshold to 0.8 (0 to 1 for low to high coherence) in order to  
153 select only highly coherent pixels in our interferograms. The 0.8 coherence threshold is used to  
154 select the pixels for the phase unwrapping step that is carried out by the Extended Minimum Cost  
155 Flow (EMCF) algorithm (*Pepe and Lanari, 2006*). By setting high values of this parameter the pixels  
156 in input to the EMCF algorithm are affected by less noise as compared to selecting low values, thus  
157 increasing the quality of the phase unwrapping step itself and reducing the noise in our final velocity  
158 maps and time-series (*De Luca et al., 2015; Cignetti et al., 2016*).

159 We also inspected the series of interferograms and excluded individual interferograms with low  
160 coherence. We identified and discarded 29 noisy interferograms in track 215A and other 11  
161 interferograms in track 437D. Finally, we applied an Atmospheric Phase Screen (APS) filtering to  
162 mitigate further atmospheric disturbances (*Hassen, 2001*). Accordingly, we used a triangular  
163 temporal filter with a width of 400 days to minimize temporal variations shorter than about a year  
164 as we focus on steady deformations rather than seasonal changes. Shorter time interval of 300 days  
165 was also tested but provided more noisy time-series.

166 The average velocity map and the incremental time-series of deformation obtained with the  
167 P-SBAS method have to be referred to a stable Reference Point. For our analysis, the reference point  
168 was initially set in the city of Massa because GPS measurements from *Bennett et al. (2012)* show  
169 that the surface velocities there are  $< 1\text{mm/yr}$ , therefore, Massa can be considered stable. Assuming

170 Massa as reference point, the average velocity map revealed the deformation pattern around the  
171 Prà di Lama lake. We then moved the reference point outside the sinkhole deformation pattern but  
172 close to ~~Pieve Fosciana town~~ (Fig. S3a). Selecting a reference point close to our study area rather  
173 than in Massa allowed us to better minimize the spatially correlated atmospheric artefacts.


174 As a final post processing step we also calculated the vertical and east-west components of the  
175 velocity field in the area covered by both the ascending and descending tracks and assuming no  
176 north-south displacement. Given that the study area is imaged by the ENVISAT satellite from two  
177 symmetrical geometries with similar incidence angles (few degrees of difference), the vertical and  
178 east-west components of the velocity field can simply be obtained solving the following system of  
179 equations (*Manzo et al., 2006*):

$$180 \quad \begin{cases} v_H = \frac{\cos \vartheta}{\sin(2\vartheta)} (v_{DESC} - v_{ASC}) = \frac{v_{DESC} - v_{ASC}}{2 \sin \vartheta} \\ v_V = \frac{\sin \vartheta}{\sin(2\vartheta)} (v_{DESC} + v_{ASC}) = \frac{v_{DESC} + v_{ASC}}{2 \cos \vartheta} \end{cases}$$

181 where  $v_H$  and  $v_V$  are the horizontal and vertical component of the velocity field,  $v_{DESC}$  and  $v_{ASC}$   
182 are the average LOS velocities in the Descending and Ascending tracks, respectively;  $\vartheta$  is the  
183 incidence angle.

184 The InSAR P-SBAS analysis shows that significant surface deformation occurs at Pieve Fosciana  
185 between 2003 and 2010. The observed deformation pattern consists of range increase mainly on  
186 the western flank of the Prà di Lama lake. The range increase is observed in both ascending and  
187 descending velocity maps (Fig. 4a, b), with average LOS velocities of up to  $-7.1 \text{ mm yr}^{-1}$  decaying to  
188  $-1 \text{ mm yr}^{-1}$  over a distance of 400 m away from the lake. Elsewhere around the lake coherence is not  
189 kept due to ground vegetation cover but few coherent pixels on eastern flank of the lake suggest  
190 that the deformation pattern may be circular, with a radius of  $\sim 600 \text{ m}$  (Fig. 4 and 5). In order to  
191 increase the number of analysed pixels we tested decreasing our coherence threshold from 0.8 to  
192 0.4. The results are displayed in Fig. S3b and show that only a few more pixels are gained north of



193 the sinkhole as compared to choosing a threshold of 0.8 (Fig. 4). We conclude that decreasing the  
194 coherence threshold does not allow to retrieve the entire deformation pattern, likely due to the fact  
195 the area is vegetated 

196 The maps of vertical and East-West velocities show vertical rates of  $-4.6 \text{ mm yr}^{-1}$  and horizontal  
197 eastward velocities of  $5.4 \text{ mm yr}^{-1}$  (Fig. 4c, d) consistent with subsidence and contraction centred at  
198 the lake. Furthermore, figure 5 shows that the current deformation pattern follows the topography,  
199 suggesting that subsidence at Prà di Lama is a long-term feature. The time-series of cumulative LOS  
200 displacements show that subsidence occurred at an approximately constant rate between ~~the~~ 2003  
201 and ~~the~~ 2008 but it slowed down in 2008 (Fig. 4e, f), indicating that subsidence at Prà di Lama occurs  
202 also between events of unrest. Furthermore, our time-series of vertical and east-west cumulative  
203 displacements also confirm that the fastest subsidence and contemporaneous eastward motion  
204 occurred until 2008 (Fig. 4 g, h). In order to better understand the mechanisms responsible for the  
205 sinkhole growth and the different types of episodic unrest we also analysed the seismicity.

### 206 3.3 Seismicity

207 ~~We analysed the seismicity~~ at the Prà di Lama lake, using the catalogue ISIDe (Italian  
208 Seismological Instrumental and Parametric Data-Base) spanning the time period from 1986 to 2016.  
209 We calculated the cumulative seismic moment release using the relation between seismic moment  
210 and magnitudes given by *Kanamori (1977)*. First, we analysed the seismic moment release and the  
211 magnitude content of the earthquakes in the area encompassing the sinkhole and the faults  
212 intersection (10 km radius, Fig. 1) to understand whether unrest at Prà di Lama is triggered by  
213 earthquakes along the active faults (Fig. 6). ~~Fig. 6a~~ shows that although several seismic swarms  
214 occurred in the area, no clear temporal correlation between the swarms and the events of unrest  
215 at Prà di Lama is observed, suggesting that the majority of seismic strain released on faults around  
216 the Prà di Lama lake does not affect the activity of the sinkhole. We removed from the plot in ~~Fig. 1~~

217 6a the large magnitude earthquake,  $M_w$  4.8, on ~~the 25<sup>th</sup>~~ of January 25, 2013 in order to better  
218 visualize the pattern of seismic moment release in time. In any case, no activity at Prà di Lama was  
219 reported in January 2013.

220 We also analysed the local seismicity around the Prà di lama lake, within a circular area of 3  
221 km radius around the lake (Fig. 1), to better understand the deformation processes occurring at the  
222 sinkhole and we found that swarms of small-magnitude earthquakes ( $M_L \leq 2$ ) occurred during both  
223 events of unrest at Prà di Lama in 1996 and 2016 (Fig. 7a, b, c), while a few earthquakes with  
224 magnitudes  $> 2$  occurred irrespective of the events of unrest. This indicates that seismicity during  
225 sinkhole activity is characterized by seismic energy released preferentially towards the small end of  
226 magnitudes spectrum. This pattern is specific of the sinkhole area as in the broader region (Fig. 6b,  
227 c) the majority of earthquakes magnitudes are in the range between  $M_L > 2$  and  $M_L < 3$  and few  $M_L$   
228  $> 3$  also occurred. We also analysed the hypocentres of the earthquakes around the Prà di lama lake  
229 (3 km radius) and find that these range between 4.5 and 11.5 km depth, indicating that deformation  
230 processes in the fault zone control the sinkhole activity. On the other hand, no earthquakes were  
231 recorded at Prà di Lama during the period of subsidence identified by InSAR between 2003 and  
232 2010, indicating that subsidence between events of unrest continues largely aseismically.

233 To strengthen our seismicity analysis and clarify whether a connection between major  
234 tectonic earthquakes and sinkhole unrest exists, we also analysed the historical parametric seismic  
235 catalogues (*Rovida et al., (2016), INGV Catalogo Parametrico dei Terremoti Italiani, CPTI15*). Figure  
236 8 shows the occurrence of major earthquakes, with magnitude  $> 4.0$  up to 20 km distant from Pieve  
237 Fosciana and the events of sinkhole unrest at Pra di lama. No clear connection between occurrence  
238 of large distant earthquakes and events of sinkhole unrest is observed, suggesting that the  
239 mechanisms responsible for activation of the Prà di Lama sinkhole should be attributed to local  
240 processes.

#### 241 4. Discussion and conclusions

242 A multi-disciplinary dataset of InSAR measurements, field observations and seismicity reveal  
243 that diverse deformation events occur at the Prà di Lama sinkhole. Two main events of sinkhole  
244 unrest occurred at Prà di Lama in 1996 and 2016 but the processes had different features. In 1996  
245 the lake-level dropped together with increased water outflow from the springs, while in 2016  
246 ground subsidence led to the expansion of the lake surface and fracturing. In 2016, fractures ~~form~~  
247 ~~in the South-Western~~ shore of the lake. The main active strike-slip fault is also oriented SW,  
248 suggesting a possible tectonic control on the deformation.

249 We also considered processes not related to the sinkhole activity that could explain the  
250 observed deformation at Prà di Lama. Active landslides can cause both vertical and horizontal  
251 surface motions (e.g. *Nishiguchi et al., 2017*). However, no landslides are identified in the deforming  
252 area around the sinkhole (Fig.3). Furthermore, the low topographic slopes rule out the presence of  
253 active landslides in the area. Concentric deformation patterns are observed above shallow aquifers  
254 (e.g. *Amelung et al., 1999*). However, deformation caused by aquifers have a seasonal pattern rather  
255 than continuous subsidence over the timespan of several years, as in ~~Prà~~ di Lama. A long-term  
256 subsidence could only be caused by over-exploitation of an aquifer but no water is pumped from  
257 the aquifers in the deforming area around ~~Prà~~ di Lama. We conclude that the observed InSAR  
258 deformation is caused by the sinkhole.

259 InSAR analysis shows that continuous but aseismic subsidence of the sinkhole occurred  
260 between the two events of unrest, during the period 2003-2010. Instead swarms of small-  
261 magnitude earthquakes coeval to the unrest events of 1996 and 2016 were recorded at depth  
262 between 4.5 and 11.5 km, indicating that a link between low magnitude seismicity and sinkhole  
263 activity exists. We suggest that seismic creep in the fault zone underneath Prà di Lama occurs,  
264 causing the diverse deformation events.

265 Seismic creep at depth could have induced pressure changes in the aquifer above the fault  
266 zone (1996 events) as well as causing subsidence by increased fracturing (2016 events). The  
267 seismicity pattern revealed by our analysis suggests that the Mt.Perpoli-T.Scoltenna strike-slip fault  
268 system underneath Prà di Lama is locally creeping, producing seismic sequences of low magnitude  
269 earthquakes. Similar seismicity patterns were observed along different active faults (i.e. *Linde et al.*  
270 *1996, Nadeau et al., 1995; Rau et al., 2007; Chen et al., 2008; Harris, 2017*). In 2006, along the  
271 Superstition Hills fault (San Andreas fault system, California) seismic creep has been favoured by  
272 high water pressure (*Wei et al., 2009; Seroliz, 1998; Harris, 2017*). We suggest that along the fault  
273 zone below Prà di Lama an increase in pressure in the aquifer in 1996 caused fracturing at the  
274 bottom of the lake and upward migration of fluids rich in clays, in agreement with the observations  
275 of lake-level drop and mud-rich water ejected by the springs in 1996. Our interpretation is also in  
276 agreement with geochemical data indicating that the high salinity of thermal waters at Prà di Lama  
277 have a deep origin, ~2000 m, where fluid circulation dissolves evaporites and carbonates, creating  
278 cavities and then reaching the surface by rapid upwelling along the faults system (*Geraudo and*  
279 *Pierotti, 2018*). The presence of deep cavities and a thick non-carbonate sequence suggests that the  
280 Prà di Lama sinkhole is a deep-sited caprock collapse sinkhole according to the sinkhole classification  
281 of *Gutiérrez et al. (2008, 2014)*. Sudden fracturing and periods of compaction of cavities created by  
282 enhanced rock dissolution and upward erosion in the fluid circulation zone could explain both  
283 sudden subsidence and fracturing, as in 2016, and periods of continuous but aseismic subsidence as  
284 in 2003-2010. Similar processes have been envisaged for the formation of a sinkhole at the  
285 Napoleonville Salt Dome, where a seismicity study suggests that fracturing enhanced the rock  
286 permeability, promoting the rising of fluids and, as a consequence, erosion and creation of deep  
287 cavities prone to collapse (*Yarushina et al., 2017; Sibson, 1996; Micklethwaite et al., 2010, Nayak*  
288 *and Dreger, 2014*). Recently, a sequence of seismic events was identified at Mineral Beach (Dead

289 Sea fault zone) and was interpreted as the result of cracks formation and faulting above subsurface  
290 cavities (Abelson et al., 2017).

291 Precursory subsidence of years to few months has been observed to precede sinkhole collapse  
292 in carbonate or evaporitic bedrocks (e.g. Baer et al., 2002; Nof et al., 2013; Cathleen and Bloom,  
293 2014; Atzori et al., 2015; Abelson et al., 2017). However, the timing of these processes strongly  
294 depends on the rheological properties of the rocks (Shalev and Lyakhovsky, 2013). Furthermore, the  
295 presence of a thick lithoid sequence in Prà di Lama may delay sinkhole collapse, also in agreement  
296 with the exceptionally long timescale (~200 years) of growth of the Prà di Lama sinkhole ( Shalev  
297 and Lykovsky, 2012; Abelson et al., 2017). However, at present we are not able to establish if and  
298 when a major collapse will occur in Prà di Lama.

299 We identified a wide range of surface deformation patterns associated with the Prà di Lama  
300 sinkhole and we suggest that a source mechanism for the sinkhole formation and growth is seismic  
301 creep in the active fault zone underneath the sinkhole. This mechanism could control the evolution  
302 of other active sinkholes in Italy as well as in other areas worldwide where sinkhole form in active  
303 fault systems (e.g. Dead Sea area). InSAR monitoring has already shown to be a valid method to  
304 detect precursory subsidence occurring before a sinkhole collapse and the recent SAR missions, such  
305 as the European Sentinel-1, will very likely provide a powerful tool to identify such deformations.

306


## 307 **References**

308 Abelson, M., Aksinenko, T., Kurzon, I., Pinsky, V., Baer, G., Nof, R., & Yechieli, Y.: Nanoseismicity forecast  
309 sinkhole collapse in the Dead Sea coast years in advance. <https://doi.org/10.1130/G39579.1>, 2017

310 Amelung, F., Galloway, D.L., Bell, J.W., Zebker, H.A., and Laczniak, R.J.: Sensing the ups and downs of Las  
311 Vegas: InSAR reveals structural control of land subsidence and aquifer-system deformation. *Geology*,  
312 27 (6), 483-486. [https://doi.org/10.1130/0091-7613\(1999\)027<0483:STUADO>2.3.CO;2](https://doi.org/10.1130/0091-7613(1999)027<0483:STUADO>2.3.CO;2), 1999

313 Atzori, S., Baer, G., Antonioli, A., & Salvi, S.: InSAR-based modelling and analysis of sinkholes along the Dead  
314 Sea coastline. *Geophysical Research Letters*, 42, 8383–8390. <https://doi.org/10.1002/2015GL066053>,  
315 2015

- 316 Baldacci, F., Botti, F., Cioni, R., Molli, G., Pierotti, L., Scozzari, A., Vaselli, L.: Geological-structural and  
 317 hydrogeochemical studies to identify seismically active structures: case history from the Equi Terme-  
 318 Monzone hydrothermal system (Northern Apennine – Italy). *Geitalia, 6th Italian Forum of Earth*  
 319 *Sciences. Rimini, 2007*
- 320 Bencini, A., Duchi, V., Martini, M.: Geochemistry of thermal springs of Tuscany (Italy). *Chemical Geology*, 19,  
 321 229-252, 1977
- 322 Baer, G., Schattner, U., Wachs D., Sandwell, D., Wdowinski, S., Frydman, S.: The lowest place on Earth is  
 323 subsiding – An InSAR (Interferometric Synthetic Aperture Radar) Perspective. *Geological Society of*  
 324 *America Bulletin*, 114 (1), 12-23. [https://doi.org/10.1130/00167606\(2002\)114<0012:TLPOEI>2.0.CO;2](https://doi.org/10.1130/00167606(2002)114<0012:TLPOEI>2.0.CO;2),  
 325 2002
- 326 Bennet, R.A., Serpelloni, E., Hreinsdottir, S., Brandon, M.T., Buble, G., Basic T., Casale, G., Cavaliere, A.,  
 327 Anzidei, M., Marjonovic, Minelli, G., Molli, G., & Montanari, A.: Syn-convergent extension observed  
 328 using the RETREAT GPS network, northern Apennines, Italy. *Journal of Geophysical Research*, 117.  
 329 <https://doi.org/10.1029/2011JB008744>, 2012
- 330 Berardino, P., Fornaro, G., Lanari, R., & Sansosti, E.: A new algorithm for surface deformation monitoring  
 331 based on Small Baseline Differential SAR interferograms. *IEEE International Geoscience and Remote*  
 332 *Sensing Symposium*, 40(11). <https://doi.org/10.1109/TGRS.2002.803792>, 2002
- 333 Bonini, M., Corti, G., Donne, D. D., Sani, F., Piccardi, L., Vannucci, G., Genco, R., Martelli, L., Ripepe, M.: Seismic  
 334 sources and stress transfer interaction among axial normal faults and external thrust fronts in the  
 335 northern Apennines (Italy): a working hypothesis based on the 1916-1920 time-space cluster of  
 336 earthquakes. *Tectonophysics*, 680, 67–89. <https://doi.org/10.1016/j.tecto.2016.04.045>, 2016
- 337 Caramanna, G., Ciotoli, G., Nisio, S.: A review of natural sinkhole phenomena in Italian plain areas. *Natural*  
 338 *Hazards*, 45, 145–172. <https://doi.org/10.1007/s11069-007-9165-7>, 2008
- 339 Castañeda, C., Gutiérrez, F., Manunta, M., Galve, J. P.: DInSAR measurements of ground deformation by  
 340 sinkholes, mining subsidence, and landslides, Ebro River, Spain. *Earth Surf. Process. Landforms*, 34, 11,  
 341 1562–1574. <https://doi.org/10.1002/esp.1848>, 2009
- 342 Casu, F., Elefante, S., Imperatore, P., Zinno, I., Manunta, M., De Luca, C., & Lanari, R.: SBAS-DInSAR parallel  
 343 processing for deformation time-series computation. *IEEE Journal of Selected Topics in Applied Earth*  
 344 *Observations and Remote Sensing*, 7(8), 3285–3296. <https://doi.org/10.1109/JSTARS.2014.2322671b>,  
 345 2014
- 346 Cathleen, J., & Blom, R.: Bayou Corne, Louisiana, sinkhole: Precursory deformation measured by radar  
 347 interferometry. *Geology*. 42 (2), 111-114. <https://doi.org/10.1130/G34972.1>, 2014
- 348 Chen, K.H., Nadeau, R.M., Rau, R.: Characteristic repeating earthquakes in an arc-continent collision  
 349 boundary zone: The Chihshang fault of eastern Taiwan. *Earth and Planetary Science Letters*.  
 350 <https://doi.org/10.1016/j.epsl.2008.09.021>, 2008
- 351 Chetoni, R.: Terme di Prà di Lama (Pieve Fosciana, Lu), indagine geognostica sulle aree dissestate nel marzo  
 352 1996. *Geological Report*, 1996
- 353 Cignetti, M., Manconi, A., Manunta, M., Giordan, D., De Luca, C., Allasia, P., Ardizzone, F.: Taking Advantage  
 354 of the ESA G-POD Service to Study Ground Deformation Processes in High Mountain Areas: A Valle  
 355 d’Aosta Case Study, Northern Italy. *Remote Sensing*, 8, 852. <https://doi.org/10.3390/rs8100852>, 2016

- 356 Closson, D.: Structural control of sinkholes and subsidence hazards along the Jordanian Dead Sea coast.  
357 *Environmental Geology*, 47 (2), 290-301. <https://doi.org/10.1007/s00254-004-1155-4>, 2005
- 358 Closson, D., Karaki, N.A., Klinger, Y., & Hussein, M. J.: Subsidence and Sinkhole Hazard Assessment in the  
359 Southern Dead Sea Area, Jordan. *Pure and Applied Geophysics*, 162, 221–248.  
360 <https://doi.org/10.1007/s00024-004-2598-y>, 2005
- 361 Rovida A., Locati M., Camassi R., Lolli B., Gasperini P.: CPTI15, the 2015 version of the Parametric Catalogue  
362 of Italian Earthquakes. Istituto Nazionale di Geofisica e Vulcanologia. [http://doi.org/10.6092/INGV.IT-](http://doi.org/10.6092/INGV.IT-CPTI15)  
363 [CPTI15](http://doi.org/10.6092/INGV.IT-CPTI15), 2016
- 364 De Luca, C., Cuccu, R., Elefante, S., Zinno, I., Manunta, M., Casola, V., Rivolta, G., Lanari, R., Casu, F.: An On-  
365 Demand Web Tool for the Unsupervised Retrieval of Earth's Surface Deformation from SAR Data: The  
366 P-SBAS Service within the ESA G-POD Environment. *Remote Sensing*, 7(11), 15630-15650.  
367 <https://doi.org/10.3390/rs71115630>, 2015
- 368 De Stefani, C.: Le Acque Termali di Pieve Fosciana. *Memorie della Società Toscana di Scienze Naturali*, 4, 72-  
369 97, 1879
- 370 Del Prete, S., Iovine, G., Parise, M., Santo, A.: Origin and distribution of different types of sinkholes in the  
371 plain areas of Southern Italy. *Geodinamica Acta* 23/1-3, 113-127. [https://doi.org/10.3166/ga.23.113-](https://doi.org/10.3166/ga.23.113-127)  
372 [127](https://doi.org/10.3166/ga.23.113-127), 2010
- 373 Di Naccio, D., Boncio, P., Brozzetti, F., Pazzaglia, F. J., & Lavecchia, G.: Morphotectonic analysis of the  
374 Lunigiana and Garfagnana grabens (northern Apennines, Italy): Implications for active normal faulting.  
375 *Geomorphology*, 201, 293–311. <https://doi.org/10.1016/j.geomorph.2013.07.003>, 2013
- 376 Doglioni, C.: A proposal for the kinematic modelling of the W-dipping subduction – possible applications to  
377 the Tyrrhenian-Apennines system. *Terra Nova*, 3, 423-434. [https://doi.org/10.1111/j.1365-](https://doi.org/10.1111/j.1365-3121.1991.tb00172.x)  
378 [3121.1991.tb00172.x](https://doi.org/10.1111/j.1365-3121.1991.tb00172.x), 1991
- 379 Elter, P., Giglia, G., Tongiorgi, M., Trevisan, L.: Tensional and compressional areas in the recent (Tortonian to  
380 Present) evolution of the Northern Apennines. *Bollettino di Geofisica Teorica ed Applicata*, 65 (8), 1975
- 381 Faccenna, C. Florindo, F., Funicello, R., Lombardi, S.: Tectonic setting and Sinkhole Features: case histories  
382 from Western Central Italy. *Quaternary Proceedings*, 3, 47–56, 1993
- 383 Faccenna, C. Becker, T.W., Miller, S.M., Serpelloni, E., & Willet, S.D.: Isostasy, dynamic topography, and the  
384 elevation of the Apennines of Italy. *Earth and Planetary Science Letters*, 407, 163–174.  
385 <https://doi.org/10.1016/j.epsl.2014.09.027>, 1993
- 386 Florea, L. J.: Using State-wide GIS data to identify the coincidence between sinkholes and geologic structure.  
387 *Journal of Cave and Karst Studies*, (August), 120–124. Retrieved from  
388 [http://digitalcommons.wku.edu/geog\\_fac\\_pub/14](http://digitalcommons.wku.edu/geog_fac_pub/14), 2005
- 389 Ford, D.C., Williams, P.: Karst Hydrogeology and Geomorphology. *Wiley, Chichester*, (562 pp.), 2007
- 390 Frumkin, A., & Raz, E.: Collapse and subsidence associated with salt karstification along the Dead Sea.  
391 *Carbonates and Evaporites*, 16(2), 117–130. [https://doi.org/https://doi.org/10.1007/bf03175830](https://doi.org/10.1007/bf03175830), 2001
- 392 **Giovanetti, F.: Pieve Fosciana Ieri e Oggi, 1975** 



- 393 Gherardi, F., Pierotti, L.: The suitability of the Pieve Fosciana hydrothermal system (Italy) as a detection site  
 394 for geochemical seismic precursors. *Applied Geochemistry*  
 395 <https://doi.org/10.1016/j.apgeochem.2018.03.009>, 2018
- 396 Gutierrez, F., Guerrero, J., Lucha, P.: A genetic classification of sinkholes illustrated from evaporite paleokarst  
 397 exposures in Spain. *Environmental Geology*, 53. <https://doi.org/10.1007/s00254-007-0727-5>, 2008
- 398 Gutierrez, F., Parise, M., De Waele J., Jourde, H.: A review on natural and human-induced geohazards and  
 399 impacts in karst. *Earth-Science Reviews*, 138. <https://doi.org/10.1016/j.earscirev.2014.08.002>, 2014
- 400 Hanssen, R. F.: Radar Interferometry: Data Interpretation and Error Analysis. Kluwer Academic Publisher.  
 401 <https://doi.org/10.1007/0-306-47633-9>, 2001
- 402 Harris, R.A.: Large earthquakes and creeping faults. *Reviews of Geophysics*, 55, 169-198.  
 403 <https://doi.org/10.1002/2016RG000539>, 2017
- 404 Harrison, R. W., Newell, W. L., & Necdet, M.: Karstification Along an Active Fault Zone in Cyprus. Atlanta,  
 405 Georgia. *U.S. Geological Survey Water-Resources Investigations Report 02-4174*, 2002
- 406 ISIDe working group version 1.0, 2016
- 407 Johnson, A. G., Kovach, R. L., & Nur, A.: Pore pressure changes during creep events on the San Andreas Fault.  
 408 *Journal of Geophysical Research*, 78 (5). <https://doi.org/10.1029/JB078i005p00851>, 1973
- 409 Kanamori, H.: The Energy Release in Great Earthquakes. *Journal of Geophysical Research*, 82(20).  
 410 <https://doi.org/10.1029/JB082i020p02981>, 1977
- 411 Kawashima, K., Aydan, O., Aoki, T., Kishimoto, I., Konagal, K., Matsui, T., Sakuta, J., Takahashi, N., Teodori, S.-  
 412 P., Yashima, A.: Reconnaissance investigation on the damage of the 2009 L'Aquila, Central Italy  
 413 earthquake. *Journal of Earthquake Engineering* 14, 817–841.  
 414 <https://doi.org/10.1080/13632460903584055>, 2010
- 415 Le Breton, E., Handy, M., Molli, G., & Ustaszewski K.: Post-20 Ma Motion of the Adriatic Plate: New  
 416 Constraints from Surrounding Orogens and Implications for Crust-Mantle Decoupling. *Tectonics*, 36.  
 417 <https://doi.org/10.1002/2016TC004443>, 2000
- 418 Linde, A.T., Gladwin M.T., Johnston, M.J.S., Gwyther, R.L. and Bilham, R.G.: A slow earthquake sequence on  
 419 the San Andreas fault. *Nature*, 383. <https://doi.org/10.1038%2F383065a0>, 1996
- 420 Manzo, M., Ricciardi, G.P., Casu F., Ventura, G., Zeni, G., Borgström S., Berardino, P., Del Gaudio, C., Lanari,  
 421 R.: Surface deformation analysis in th Ischia Island (Italy) based on spaceborne radar interferometry.  
 422 *Journal of Volcanology and Geothermal Research* 151, 399-416.  
 423 <https://doi.org/10.1016/j.jvolgeores.2005.09.010>, 2006
- 424 Meletti, C., Patacca, E., & Scandone P.: Construction of a Seismotectonic Model: The Case of Italy. *Pure and*  
 425 *applied Geophysics*, 157, 11-35. <https://doi.org/10.1007/PL00001089>, 2000
- 426 Micklethwaite, S., Sheldon, H. A., & Baker, T.: Active fault and shear processes and their implications for  
 427 mineral deposit formation and discovery. *Journal of Structural Geology*, 32(2), 151–165.  
 428 <https://doi.org/10.1016/j.jsg.2009.10.009>, 2010
- 429 Molli, G., Torelli, L., & Storti, F.: The 2013 Lunigiana (Central Italy) earthquake: Seismic source analysis from



- 430 DInSar and seismological data, and geodynamic implications for the northern Apennines. A discussion.  
 431 *Tectonophysics*, 668–669, 108–112. <http://dx.doi.org/10.1016/j.tecto.2015.07.041>, 2016  
 432
- 433 Molli, G., Pinelli, G., Bigot, A., Bennett R., Malavieille J., Serpelloni E.: Active Faults in the inner northern  
 434 Apennines: a multidisciplinary reappraisal. From 1997 to 2016: Three Destructive Earthquakes along  
 435 the Central Apennine Fault system, Italy. July 19<sup>th</sup>-22<sup>nd</sup> 2017 Camerino, Volume Abstract, 2017
- 436 Nadeau, R.M., Foxal, W., McEvelly, T.V.: Clustering and Periodic Recurrence of Microearthquakes on the San  
 437 Andreas Fault at Parkfield, California. *Science*, 267. <https://doi.org/10.1126/science.267.5197.503>,  
 438 1995
- 439 Nayak, A., & Dreger, D. S.: Moment Tensor Inversion of Seismic Events Associated with the Sinkhole at  
 440 Napoleonville Salt Dome, Louisiana. *Bulletin of the Seismological Society of America*, 104(4), 1763–  
 441 1776. <https://doi.org/10.1785/0120130260>, 2014
- 442 Neuendorf, K., Mehl, J., Jackson, J.: Glossary of geology, 5th edn. *American Geological Institute*, 779 pp., 2005
- 443 Nishiguchi, T., Tsuchiya, S., Imaizumi, F.: Detection and accuracy of landslide movement by InSAR analysis  
 444 using PALSAR-2 data. *Landslides*, 14:1483–1490. <https://doi.org/10.1007/s10346-017-0821-z>, 2017
- 445 Nisio, S.: The sinkholes in Tuscany Region. *Memorie Descrittive Carta Geologica d'Italia LXXXV*, 2008
- 446 Nof, R. N., Baer, G., Ziv, A., Raz, E., Atzori, S., & Salvi, S.: Sinkhole precursors along the Dead Sea, Israel,  
 447 revealed by SAR interferometry. *Geology*, 41, (9), 1019-1022. <https://doi.org/10.1130/G34505.1>, 2013
- 448 Parise, M., Perrone, A., Violante, C., Stewart, J.P., Simonelli, A., Guzzetti, F.: Activity of the Italian National  
 449 Research Council in the aftermath of the 6 April 2009 Abruzzo earthquake: the Sinizzo Lake case study.  
 450 *Proc. 2nd Int. Workshop "Sinkholes in the Natural and Anthropogenic Environment", Rome, pp.*  
 451 <http://doi.org/623-641.10.13140/2.1.3094.1127>, 2010
- 452 Parise, M. and Vennari, C.: A chronological catalogue of sinkholes in Italy: the first step toward a real  
 453 evaluation of the sinkhole hazard. In: Land L, Doctor DH, Stephenson JB, editors. 2013. *Sinkholes and*  
 454 *the Engineering and Environmental Impacts of Karst: Proceedings of the Thirteenth Multidisciplinary*  
 455 *Conference, May 6-10, Carlsbad, New Mexico: NCKRI Symposium 2.* Carlsbad (NM): National Cave and  
 456 Karst Research Institute. <http://doi.org/10.5038/9780979542275.1149>, 2013
- 457 Patacca, E., & Scandone, P.: Post-Tortonian mountain building in the Apennines, the role of the passive  
 458 sinking of a relic lithospheric slab. *The Lithosphere in Italy*, 157–176, 1989
- 459 Pepe, A. and Lanari, R. On the extension of the minimum cost flow algorithm for phase unwrapping of  
 460 multitemporal differential SAR interferograms. *IEEE Transaction in Geoscience and Remote Sensing*, 44,  
 461 9, 2374–2383. <http://doi.org/10.1109/TGRS.2006.873207>, 2006
- 462 Pezzo, G., Boncori, J.P.M., Atzori, S., Piccinini, D., Antonioli, A., Salvi, S.: The 2013 Lunigiana (Central Italy)  
 463 earthquake: Seismic source analysis from DInSAR and seismological data, and geodynamical implications  
 464 for the northern Apennines. *Tectonophysics* 636, 315–324.  
 465 <http://dx.doi.org/10.1016/j.tecto.2014.09.005>, 2014  
 466
- 467 Pinelli, G.: Tettonica recente e attiva nell'Appennino interno a Nord dell'Arno: una revisione delle strutture e  
 468 delle problematiche. Diploma Thesis (89 pp), 2013
- 469 Raffaelli, R.: Sulle acque termali di Pieve Fosciana, 1869

- 470 Rau, R., Chen, K.H., Ching, K.: Repeating earthquakes and seismic potential along the northern Longitudinal  
471 Valley fault of Taiwan. *Geophysical Research Letters*, 34. <http://doi.org/10.1029/2007GL031622>, 2007
- 472 Rovida A., Locati M., Camassi R., Lolli B., Gasperini P.: CPTI15, the 2015 version of the Parametric Catalogue  
473 of Italian Earthquakes. *Istituto Nazionale di Geofisica e Vulcanologia*. [http://doi.org/10.6092/INGV.IT-](http://doi.org/10.6092/INGV.IT-CPTI15)  
474 [CPTI15](http://doi.org/10.6092/INGV.IT-CPTI15), 2016
- 475 Salamon, A.: Seismically induced ground effects of the February 11, 2004, M L = 5.2, North-eastern Dead Sea  
476 earthquake. *Geological Survey of Israel Report*, 2004
- 477 Santo, A., Del Prete, S., Di Crescenzo, G., and Rotella M.: Karst processes and slope instability: some  
478 investigations in the carbonate Apennine of Campania (southern Italy). In: Parise, M., Gunn, J. (Eds.),  
479 Natural and Anthropogenic Hazards in Karst Areas: Recognition, Analysis, and Mitigation. *Geological*  
480 *Society, London*, 279, pp. 59–72. <http://doi.org/10.1144/SP279.60305-8719/07>, 2007
- 481 Serpelloni, E., Anzidei, M., Baldi, P., Casula, G., & Galvani, A.: Crustal velocity and strain -rate fields in Italy  
482 and surrounding regions: New results from the analysis of permanent and non-permanent GPS  
483 networks. *Geophysical Journal International*, 161(3), 861–880. [https://doi.org/10.1111/j.1365-](https://doi.org/10.1111/j.1365-246X.2005.02618.x)  
484 [246X.2005.02618.x](https://doi.org/10.1111/j.1365-246X.2005.02618.x), 2005
- 485 Shalev, E., & Lyakhovsky, V.: Viscoelastic damage modeling of sinkhole formation. *Journal of Structural*  
486 *Geology*, 42, 163–170. <https://doi.org/10.1016/j.jsg.2012.05.010>, 2012
- 487 Scholz, C. H.: Earthquakes and friction laws. *Nature*, 391, 37–42. <https://doi.org/10.1038/34097>, 1998
- 488 Sibson, R. H.: Roughness at the Base of the Seismogenic Zone: Contributing Factors. *Journal of Geophysical*  
489 *Research*, 87 (B7), 5791-5799. <https://doi.org/10.1029/JB089iB07p05791>, 1984
- 490 Sibson, R. H.: Structural permeability of fluid-driven fault-fracture meshes. *Journal of Structural Geology*, 18  
491 (8),1031-1042. [https://doi.org/10.1016/0191-8141\(96\)00032-6](https://doi.org/10.1016/0191-8141(96)00032-6), 1996
- 492 Stramondo, S., Vannoli, P., Cannelli, V., Polcari, M., Melini, D., Samsonov, S., Moro, M., Bignami, C., & Saroli,  
493 M.: X- and C-band SAR surface displacement for the 2013 Lunigiana earthquake (Northern Italy): a  
494 breached relay ramp? *IEEE J. Sel. Top. Appl. Earth Obs. Remote Sens.*  
495 <http://dx.doi.org/10.1109/JSTARS.2014.2313640>, 2014
- 496 Tertulliani, A., & Maramai, A.: Macroseismic evidence and site effects for the Lunigiana (Italy) 1995  
497 Earthquake. *Journal of Seismology*, 2 (3), 209–222. <https://doi.org/10.1023/A:1009734620985>, 1998
- 498 Vannoli, P.: Il terremoto in Garfagnana del 25 gennaio 2013 visto dal geologo. Retrieved from  
499 [https://ingvterremoti.wordpress.com/2013/02/06/il-terremoto-del-25-gennaio-2013-visto-dal-](https://ingvterremoti.wordpress.com/2013/02/06/il-terremoto-del-25-gennaio-2013-visto-dal-geologo/#more-3132)  
500 [geologo/#more-3132](https://ingvterremoti.wordpress.com/2013/02/06/il-terremoto-del-25-gennaio-2013-visto-dal-geologo/#more-3132), 2013
- 501 Wadas, S. H., Tanner, D. C., Polom, U., & Krawczyk, C. M.: Structural analysis of S-wave seismics around an  
502 urban sinkhole; evidence of enhanced suberosion in a strike-slip fault zone. *Natural Hazards and Earth*  
503 *System Sciences*. <https://doi.org/10.5194/nhess-2017-315>, 2017
- 504 Wei, M., Sandwell, D., & Fialko, Y.: A silent Mw 4.7 slip event of October 2006 on the Superstition Hills fault,  
505 southern California. *Journal of Geophysical Research*, 114, <https://doi.org/10.1029/2008JB006135>,  
506 2009

507 Yarushina, V. M., Podladchikov, Y.Y., Minakov, A., & Räss, L.: On the Mechanisms of Stress-Triggered Seismic  
508 Events during Fluid Injection. *Sixth Biot Conference on Poromechanics, American Society of Civil*  
509 *Engineers*. <https://doi.org/10.1061/9780784480779.098>, 2017

510

511

512

513

514

515

516

517

518

519

520

521

522

523

524

525

526

527

528

529

530

531

532

533

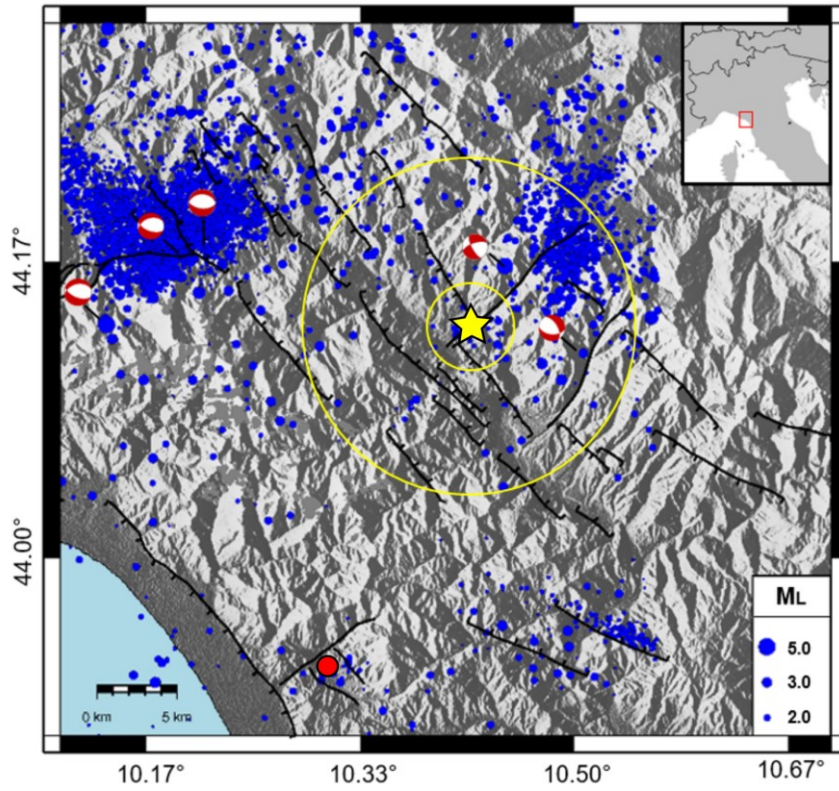
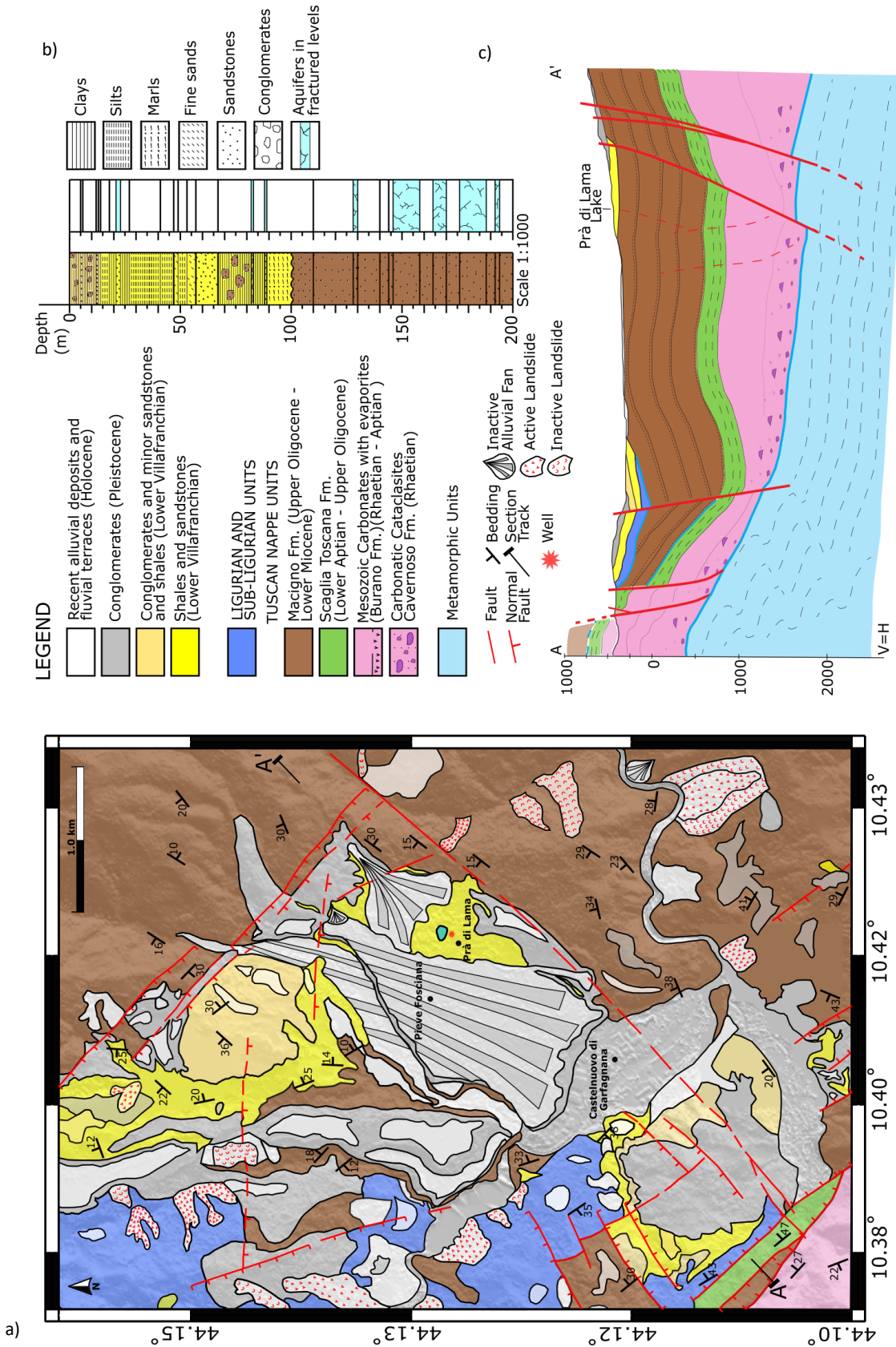


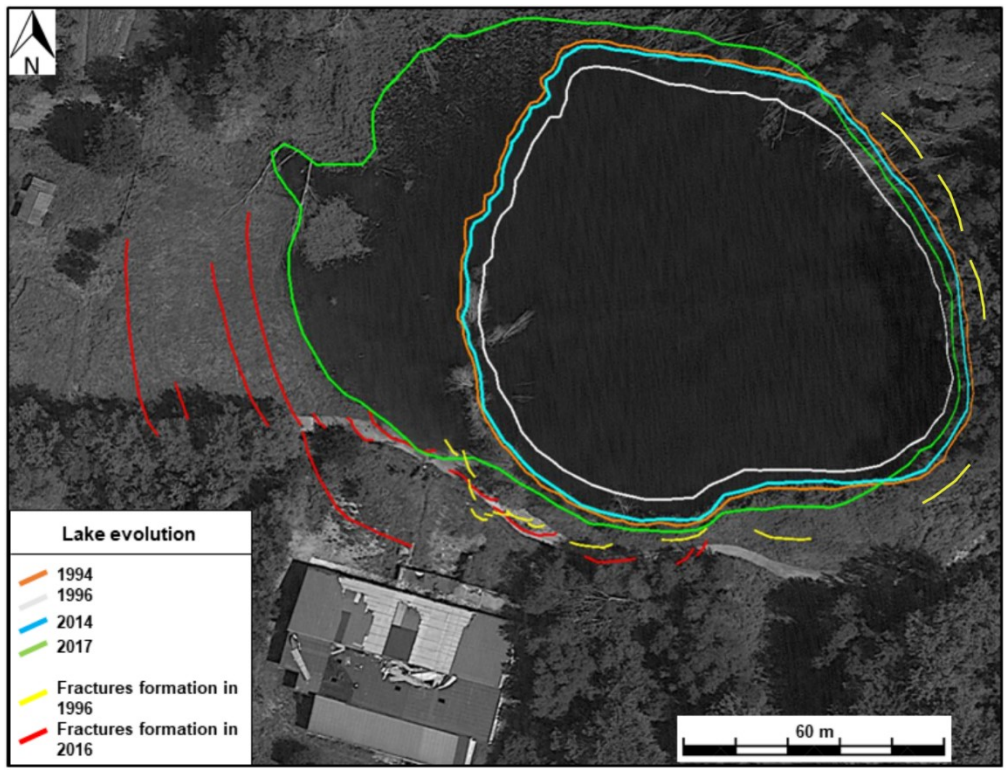
**Figure 1 - Study area.** The Prà di Lama sinkhole is marked by the yellow star. Black tick lines are faults. Blue dots are the earthquakes between 1986 and 2017. Focal mechanisms are from the Regional Centroid Moment Tensor (RCMT) catalogue. The yellow circles represent the areas with radii of 3km and 10 km used for the seismicity analysis. The red dot is the sinkhole of Camaiore (*Caramanna et al. 2008*). The red box in the *inset* marks the location of the area shown in the main figure.



553  
554  
555  
556  
557

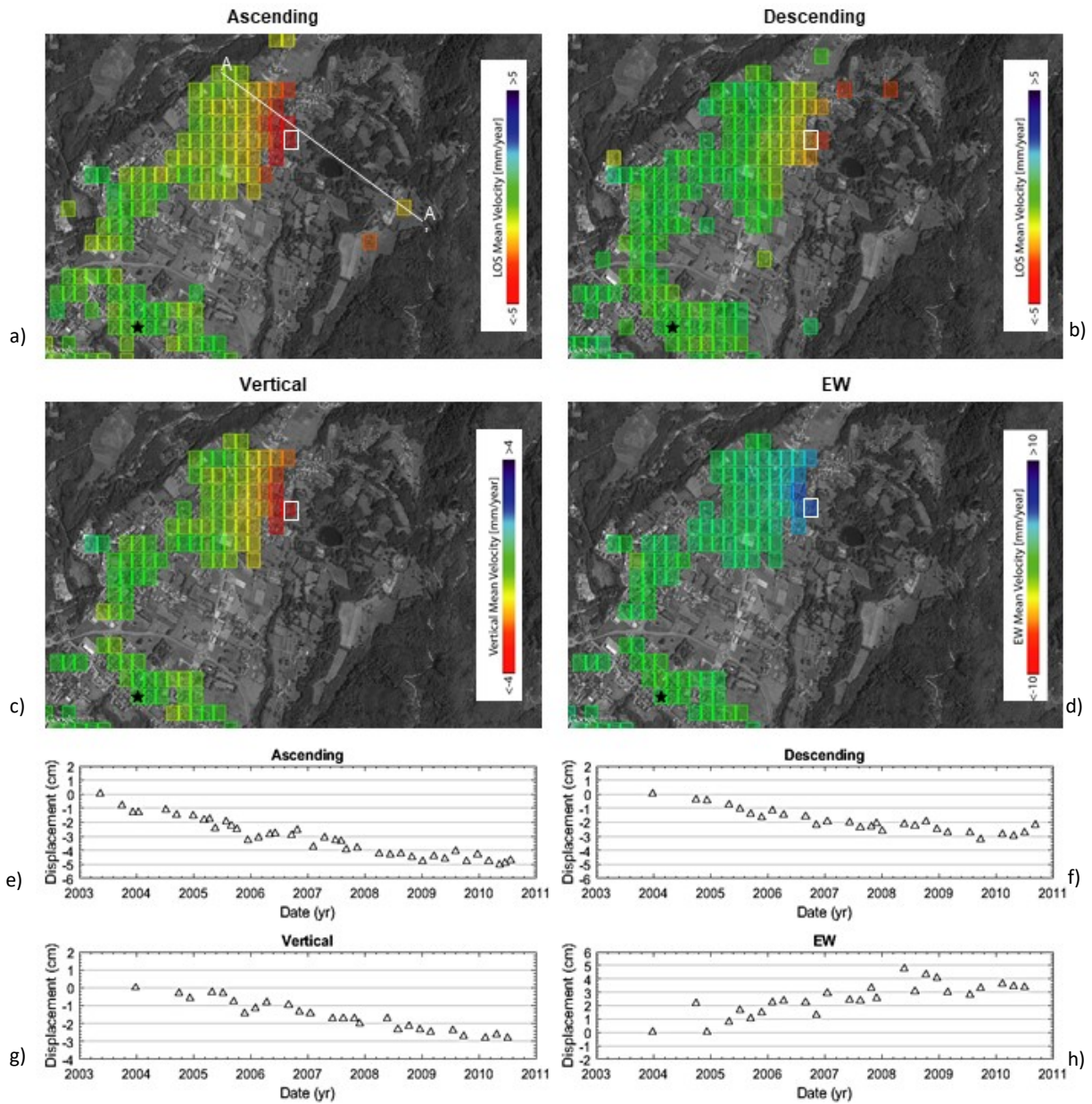
**Figure 2 – Geological setting of the study area. a)** Geological, structural and geomorphological map of the area nearby Prà di Lama showing the main tectonic and lithostratigraphic units. **b)** Schematic sedimentary sequence of the Villafranchian deposits obtained from the well drilled at Prà di Lama (Modified from Chetoni 1995). **c)** Stratigraphic cross-section across the Garfagnana graben.





558  
559  
560

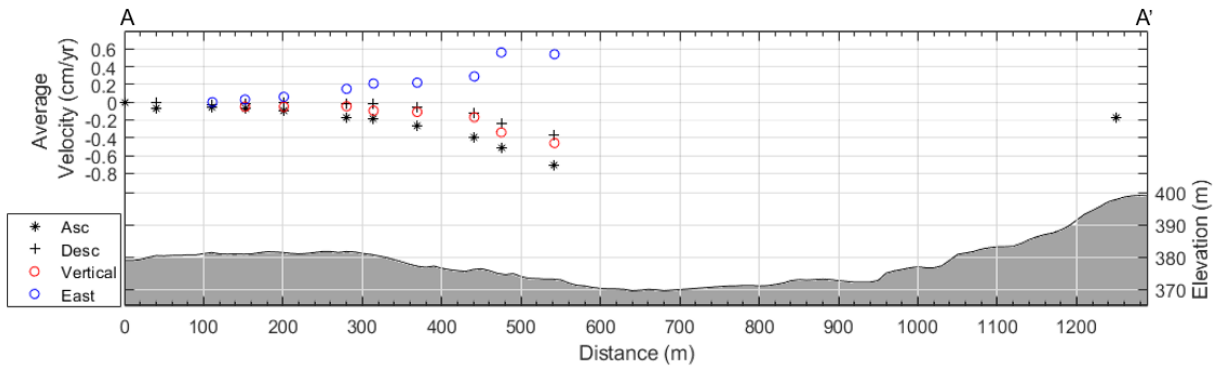
**Figure 3 – Evolution of the Prù di Lama lake between 1994 and 2017.** Lake shores variation have been retrieved from the analysis of Landsat image



561  
562

563 **Figure 4 – a, b)** Maps of average surface velocity and its vertical (c) and East-West (d) components obtained from ENVISAT SAR images  
 564 acquired between 2003 and 2010. Negative values indicate range increase. The white line in panel a) marks the cross-section shown in figure 4.  
 565 The black star is the point used as reference for the InSAR-SBAS processing. e, f, g, h) Time-series of incremental  
 566 deformation extracted from the pixel bounded with the white rectangle.

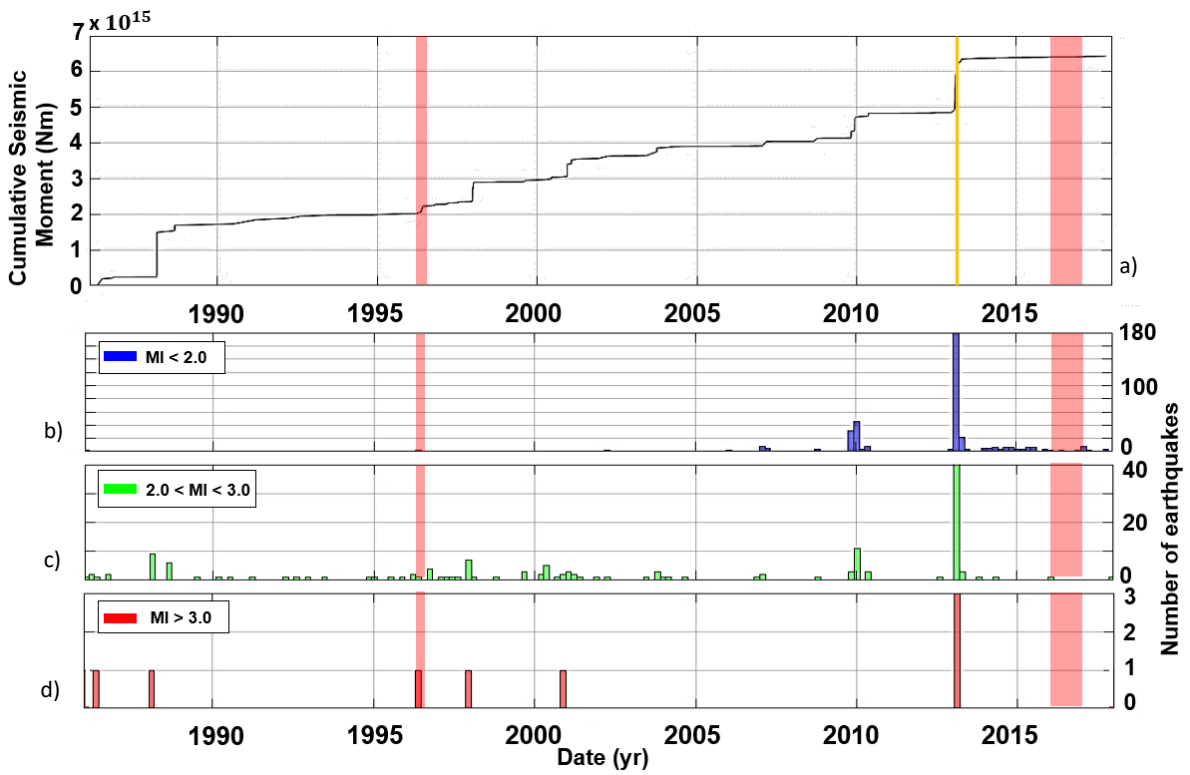
567



568

569 **Figure 5 - Cross-section of topography and InSAR velocities along the A-A' profile as shown in figure 3a.**

570

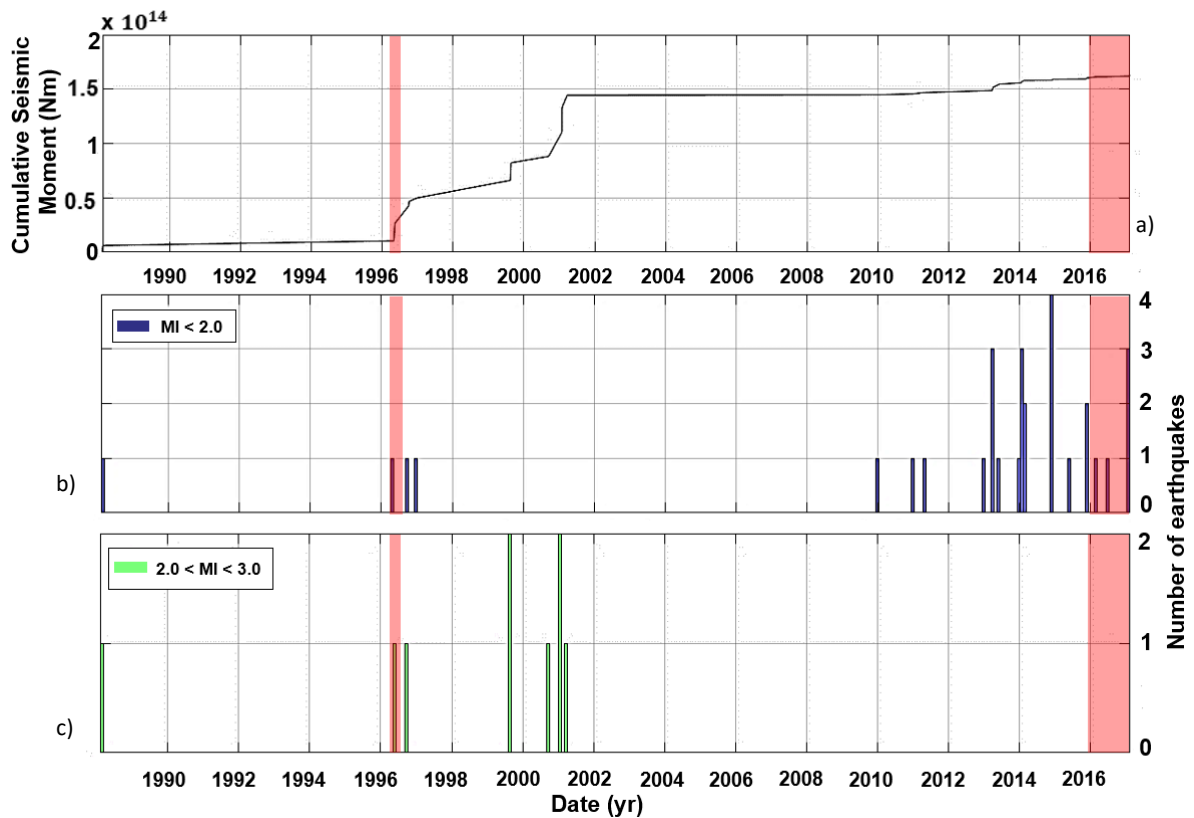


571

572 **Figure 6 – Seismicity features of an area 10 km in radius around the Prà di Lama lake.** Cumulative seismic moment released in the  
 573 area (a) and histograms of the number of earthquakes per month. Three different classes of magnitude have been created: MI < 2.0  
 574 (b), 2.0 < MI < 3.0 (c) and MI > 3.0 (d). The dataset covers the period between 1986 and 2017. The red transparent bars indicate the  
 575 two events of unrest of 1996 and 2016.

576





577  
578  
579  
580  
581

**Figure 7 - Seismicity features of an area 3 km in radius around the Prà di Lama lake.** Plot of the cumulative seismic moment released in the area (a) and histograms showing the number of earthquakes occurred each month. Two different classes of Magnitude have been created:  $MI < 2.0$  (b),  $2.0 < MI < 3.0$  (c). No events of  $MI > 3.0$  occurred in the area between 1986 and 2017. The red transparent bars indicate the two events of unrest of 1996 and 2016.

582  
583

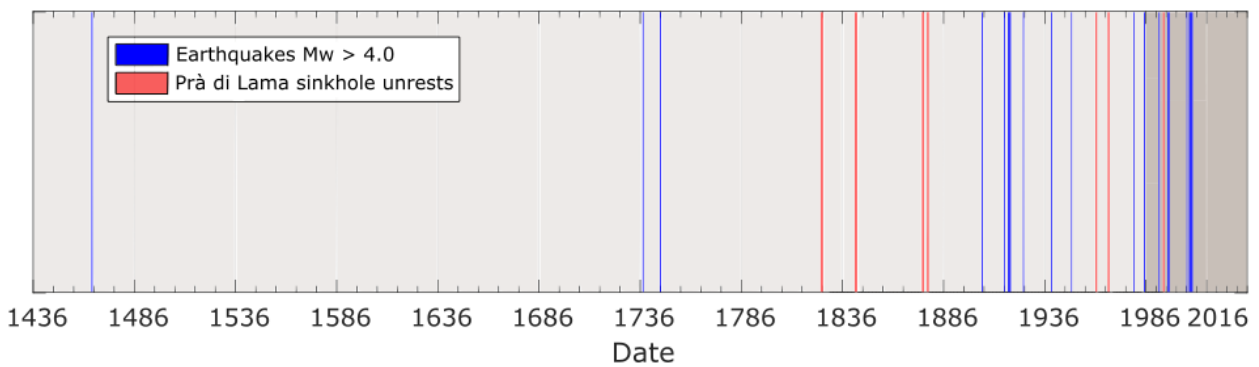


**Figure 8 – Comparison between the earthquakes (blue lines) in the Garfagnana area (INGV Catalogo Parametrico dei Terremoti Italiani CPT115, Rovida et al., 2016), and events of unrest at the Prà di Lama sinkhole (red lines).**

586  
587  
588  
589

<b>Year</b>	<b>Brief description of the event</b>
<b>991</b>	Seasonal pool fed by springs
<b>1828</b>	Bursts of the springs water flow. Uprising of muddy waters and clays ( <i>Raffaelli, 1869; De Stefani, 1879</i> )
<b>1843</b>	Bursts of the springs water flow. Uprising of muddy waters and clays ( <i>Raffaelli, 1869; De Stefani, 1879</i> )
<b>1876</b>	Subsidence and fracturing ( <i>De Stefani, 1879</i> )
<b>1877</b>	Subsidence and fracturing ( <i>De Stefani, 1879</i> )
<b>1962</b>	Bursts of the spring water flow. Uprising of muddy waters and clays ( <i>Giovannetti, 1975</i> )
<b>1969</b>	Abrupt falling of the water level and fracturing along the shores. The lake almost disappeared ( <i>Giovannetti, 1975</i> )
<b>1985</b>	Arising of muddy waters in a well
<b>1996</b>	Abrupt fall of the water level and fracturing along the shores
<b>2016-2017</b>	Subsidence and fracturing

591 **Table 1 – Description of the activity at Prà di Lama lake**